Torque Vectoring Algorithm of Electronic-Four-Wheel Drive Vehicles for Enhancement of Cornering Performance

Giseo Park, Kyoungseok Han, *Member, IEEE,* Kanghyun Nam, *Member, IEEE,* Heeseong Kim, and Seibum B. Choi, *Member, IEEE*

***Abstract*—This paper introduces a new torque vectoring (TV) algorithm with regards to enhancing the cornering performance of the electronic-four-wheel drive (e-4WD) vehicles. The proposed TV algorithm aims to distribute the in-wheel motor (IWM) torques to the left and right wheels assisting the vehicle in following the driver's intended trajectories. The proposed TV algorithm first included a yaw rate controller reference for neutral-steering which leads to the improvement of vehicle cornering agility. Thereafter, in-vehicle sensors and a standalone global positioning system (GPS) combined with a smooth sliding mode controller (SMC) were used based on a vehicle bicycle model to generate desired yaw moment values to track the reference. Finally, a novel torque distribution algorithm using the Daisy-chaining allocation, which is suitable for redundant actuator configuration, was utilized. Noteworthy, the Daisy-chaining allocation algorithm takes into account a torque operation area with maximum IWM torque. In this manner, based on the vehicle bicycle model and using the CARSIM interface, the simulations, evaluation and verifications of the proposed control technique were done. Thereafter, considering a real-car based experiments with various driving scenarios, the effectiveness of the proposed TV algorithm was evaluated. It was confirmed that some evaluation factors in terms of the cornering performance were improved. The following main contributions makes the proposed TV algorithm be a meaningful solution to enhance the cornering performance of e-4WD vehicles: 1) improvement of both smoothness and convergence rate of control action, 2) a practical and intuitive way to distribute IWM torques, and 3) high applicability to mass-produced vehicles.**

***Index Terms*— Torque vectoring, electronic-four-wheel drive system, sliding mode controller, in-wheel motor, Daisy-chaining allocation**

I. INTRODUCTION

A TV system of a vehicle, which varies torques to each wheel independently, aims at both improved traction and handling performances [1]. The difference between left and right hand side torques by this TV system can assist the vehicle in following the driver's intended line. In keeping with consumers' growing demand for high-performance vehicles, TV system is considered a beneficial chassis control system for vehicle cornering performance [2].

To overcome some limitations of the already mass-produced active differentials for TV system (e.g. slow response time and environmental friendliness [3]), electric drivetrains have been widely investigated [4]. Over the last few decades, several automobile companies have introduced IWMs with many advantages [5]. 1) The precise torque generation from IWM improves the performance of chassis control systems, such as anti-lock brake systems and traction control systems. 2) Both forward and reverse torques can be generated. 3) High transfer efficiency of IWM torque is possible due to the absence of mechanical backlash and compliance effects of the driveshaft [5, 6]. These advantages motivate the use of IWM in TV system.

In previous papers, state-of-the-art TV algorithms are suggested. In [1], an allocation algorithm for optimal torque distribution is proposed. However, an offline optimization procedure has to be involved in this logic. In [2], integration of yaw rate and sideslip controllers based on the phase-plane analysis is suggested to allow sustained high values of the sideslip angle. Also, an algorithm with the constrained optimization of tire force is found in [7]. However, the feedback errors from the estimated sideslip angle may cause stability issues in these algorithms. An integral SMC which is supposed to be robust to tire model uncertainty is developed in [8], but it may have to worry about chattering issues of SMC. An optimal torque vectoring based on the linear matrix inequality is presented in [9]. However, the computational burden problem may arise in this algorithm. In [10], an algorithm involving the human behavior model is suggested, but it requires a large amount of road preview data. Also, TV algorithms based on a proportional-integral (PI) feedback controller with feedforward term are proposed in [11] and [12], but, the torque distribution method considering the limit value of IWM torque is not presented.

Considering the limitations of these previous studies, the goal of this paper is the development of a practical TV algorithm. Also, the proposed algorithm is mainly aimed at improving the

G. Park and S. B. Choi are with the Department of Mechanical Engineering, Korea Advanced Institute of Science and Technology (KAIST), Daejeon 34141, Korea (e-mail: giseo123@kaist.ac.kr; sbchoi@kaist.ac.kr).

K, Han is with the Department of Aerospace Engineering, University of Michigan, Ann Arbor 48109, USA (e-mail:kyoungsh@umich.edu).

K, Nam is with the Department of Mechanical Engineering, Yeungnam University, Gyeongsan 38451, Korea (e-mail:khnam@yu.ac.kr).

H, Kim is with the Department of Automotive Systems Engineering, University of Michigan-Dearborn, Dearborn 48128, USA (e-mail:castlek@umich.edu).

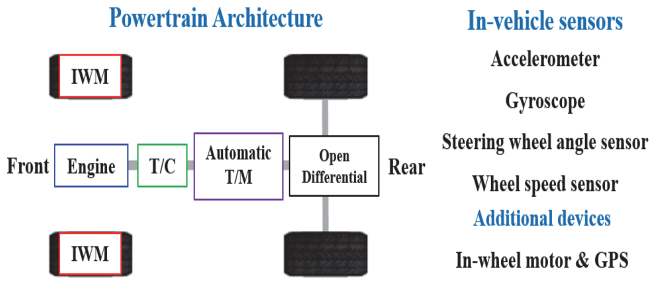

Fig. 1. Overall system configuration.

cornering performance on the road surface of high tire-road friction coefficient (TRFC), such as dry asphalt.

The overall system configuration is illustrated in Fig. 1. The target vehicle is an e-4WD system that two IWMs of the front wheels coexist with mechanical driveline devices (the internal combustion engine, the automatic transmission, and the open differential). Some easily available in-vehicle sensors are utilized, and a standalone GPS to measure the vehicle longitudinal velocity is additionally included in the sensor configuration.

A control target, yaw rate reference leads to neutral-steer characteristics so that the driver's fun-to-drive can be attained in a quantitative aspect while improving the vehicle cornering agility [13, 14]. The novelty distinguishing the suggested algorithm from the previous torque vectoring algorithms is the development of both smooth SMC for yaw rate control and new torque distribution method based on Daisy-chaining allocation. Accordingly, the main contributions are summarized as follows. 1) Smooth SMC with the feed-forward term actively reflecting the yaw rate reference improves both convergence rate of control action and vehicle cornering agility. 2) Novel Daisy-chaining allocation to distribute IWM torques is practical and intuitive method aimed at real-car application. In particular, it elaborately reflects both the characteristics of IWM and the tire friction circle. 3) Thanks to simple structure, the overall algorithm can be easily implemented with very little computational burden.

This paper is comprised of seven sections. In Section II, the vehicle bicycle model is described. Section III deals with the controller design. To follow the desired yaw moment, the torque distribution algorithm is developed in Section IV. Also, simulation and experiment results are evaluated to validate the proposed algorithm in Sections V and VI, respectively. Lastly, the conclusions of this paper are presented in Section VII.

II. Vehicle Bicycle Model

In this section, the vehicle bicycle model considering the vehicle dynamics on only the yaw plane are introduced. As shown in Fig. 2 (a), the bicycle model (also called the single-track model) combines the tire forces of both sides at the center line [15]. Thus, the left and right tire forces are not considered separately in this vehicle model. Since the wheels are assumed to be located at the center line, the lumped lateral tire forces, i.e. $F_{yf}(= F_{y,fl} + F_{y,fr})$ and $F_{yr}(= F_{y,rl} + F_{y,rr})$ are expressed in the front and rear tire coordinate frames,

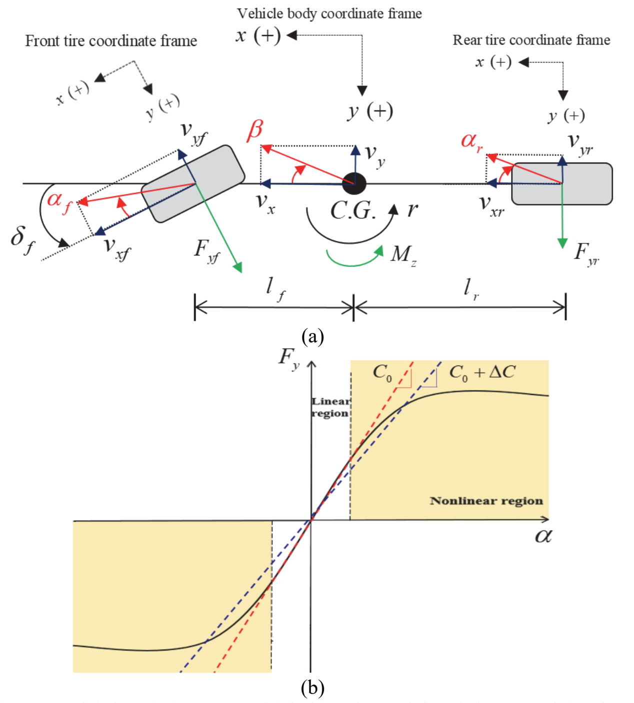

Fig. 2. Model description: (a) Vehicle bicycle model and (b) Lateral tire force model.

respectively. Also, in the vehicle body coordinate frame, the moment and lateral force balance equations are derived as

$$I_z \dot{r} = F_{yf} l_f - F_{yr} l_r + M_z \tag{1}$$

$$m a_y = F_{yf} + F_{yr} \tag{2}$$

where the lateral acceleration at the vehicle center of gravity (CG) a_y is

$$a_y = \dot{v}_y + r v_x . \tag{3}$$

Here, I_z is the vehicle yaw moment of inertia; r vehicle yaw rate; M_z the additional yaw moment; and m the total mass of the vehicle. Also, v_x and v_y are the vehicle longitudinal and lateral velocities; and l_f and l_r the CG-front and CG-rear axle distances, respectively: $L = l_f + l_r$.

In case of the small vehicle sideslip angle $\beta\,(= tan^{-1}(v_y/v_x) \approx v_y/v_x)$, the front and rear tire slip angles α_f and α_r in tire coordinate frames are defined as follows:

$$\begin{bmatrix} \alpha_f \\ \alpha_r \end{bmatrix} = \begin{bmatrix} \tan^{-1}\left(v_{yf} / v_{xf}\right) \\ \tan^{-1}\left(v_{yr} / v_{xr}\right) \end{bmatrix} \approx \begin{bmatrix} \beta + l_f r / v_x - \delta_f \\ \beta - l_r r / v_x \end{bmatrix}. \tag{4}$$

Here, δ_f is the front steering angle converted from the steering wheel angle δ_{SWA} with a constant gear ratio GR_s. Assuming that the lateral tire forces are linearly proportional to the tire slip angles ($F_{yf} = -C_f \alpha_f$ and $F_{yr} = -C_r \alpha_r$) and v_x changes slowly (i.e. $\dot{\beta} \approx \dot{v}_y / v_x$), the state space forms of the bicycle model are derived from Eqs. (1)-(4):

$$\dot{\beta} = -\frac{C_f + C_r}{m v_x}\beta + \left(\frac{C_r l_r - C_f l_f}{m v_x^2} - 1\right) r + \frac{C_f}{m v_x}\delta_f \tag{5}$$

$$\dot{r} = \frac{C_r l_r - C_f l_f}{I_z}\beta - \frac{C_f l_f^2 + C_r l_r^2}{I_z v_x} r + \frac{C_f l_f}{I_z}\delta_f + \frac{M_z}{I_z} \tag{6}$$

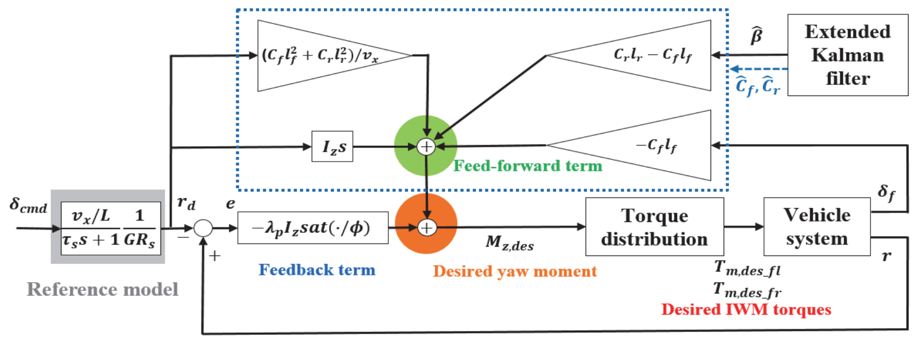

Fig.3. Block diagrams of the overall algorithm.

where C_f and C_r are, respectively, the tire cornering stiffness values of the front and rear axles. As shown in Fig. 2 (b), C_* can be expressed as the sum of nominal part C_{*0} and unknown variable ΔC_*. Generally, the steady state of the bicycle model is considered the yaw rate reference of vehicle cornering (i.e. $\dot{\beta} = 0$ in Eq. (5) and $\dot{r} = 0$ and $M_z = 0$ in Eq. (6)). It includes the driver's steering and velocity commands as well as the under-steer gradient [16, 17]:

$$r_{ss,bic} = \frac{v_x}{L + K_v v_x^2} \delta_f \tag{7}$$

where the under-steer gradient is

$$K_v = \frac{m(l_r C_r - l_f C_f)}{L C_f C_r} = \frac{\partial \delta_f}{\partial a_y}. \tag{8}$$

According to the value of K_v, the steering characteristics at the steady state cornering can be classified ($K_v > 0$: under-steering ($|\alpha_f| > |\alpha_r|$), $K_v = 0$: neutral-steering ($|\alpha_f| = |\alpha_r|$), and $K_v < 0$: over-steering ($|\alpha_f| < |\alpha_r|$) [10, 18].

III. Controller Design

The block diagrams of the overall algorithm are illustrated in Fig. 3. Here, the extended Kalman filter (EKF) based on the bicycle model having the state vector $[\beta \quad r \quad \Delta C_f \quad \Delta C_r]$ is utilized to estimate the sideslip angle $\hat{\beta}$ (detailed explanations are introduced in [15]). Since the unknown variables ΔC_* are simultaneously estimated by this EKF, the estimated cornering stiffness values of the front and rear axles can be utilized:

$$\hat{C}_f = C_{f0} + \Delta \hat{C}_f \tag{9}$$

$$\hat{C}_r = C_{r0} + \Delta \hat{C}_r. \tag{10}$$

A. Reference Model

Due to safety issues, most commercial vehicles should never be designed to have over-steer characteristics at the steady state cornering [16]. For this reason, some yaw rate controllers select $r_{ss,bic}$ in Eq. (7) with a positive K_v as a reference model [3, 6, 7, 10, 16]. On the other hand, to allow slightly more aggressive cornering, the yaw rate reference aims to be close to the neutral-steer characteristics ($K_v \to 0$) in this paper. Therefore, it is expected that the difference between slip angles of the front and rear tires can certainly be reduced. With the first order filter reflecting the time lag of the steering apparatus, the yaw rate reference is derived as the following equation:

$$r_d(s) = \frac{v_x}{L(\tau_s s + 1)} \frac{\delta_{cmd}}{GR_s} \tag{11}$$

with $|r_d| \le \mu g / v_x$.

Here, τ_s is the time constant parameter (by analyzing the time delay between r and δ_{cmd}, $\tau_s = 0.05$ s is chosen in this paper). The reference in Eq. (11) is completely free from the value of tire cornering stiffness. The estimation of TRFC μ is introduced in many existing research (e.g. dynamic-based methods [19, 20], and combined slip-based methods [21, 22]).

B. Smooth Sliding Mode Controller

The striking feature of SMC is its robustness with respect to unmodeled dynamics, parametric uncertainties and external disturbances [23]. However, the chattering issue of general SMC makes the vehicle ride comfort deteriorate severely in real-car application (the chattering issue also has an adverse effect on the durability of IWM systems). Hence, the smooth SMC proposed in this section replaces the signum function sgn(·) of the general SMC with the saturation function sat(·). To track the yaw rate reference, the smooth SMC is designed as the following. Firstly, consider the sliding variable:

$$e = r - r_d. \tag{12}$$

Then, let $\dot{e}$ be the saturation function as follows:

$$\dot{e} = -\lambda_P sat(e/\phi) \tag{13}$$

where

$$sat(e/\phi) = \begin{cases} 1 & (\phi < e) \\ e/\phi & (-\phi \le e \le \phi) \\ -1 & (e < -\phi) \end{cases}.$$

At this point, λ_P is the positive proportional gain of the feedback term and ϕ is the positive saturation boundary of the sliding variable, respectively. From the derivative of Eq. (12), the error dynamics can be rewritten as follows.

$$\dot{e} = \frac{C_r l_r - C_f l_f}{I_z} \beta - \frac{C_f l_f^2 + C_r l_r^2}{I_z v_x} r + \frac{C_f l_f}{I_z} \delta_f - \dot{r}_d + \frac{M_z}{I_z} + \frac{M_{z,unc}(r, \beta, \delta_f)}{I_z} \tag{14}$$

Here, $M_{z,unc}$, a function of r, β and δ_f is an uncertainty part of yaw moment mainly composed of lateral tire forces, self-aligning torques, and external disturbances. From the analysis in extreme driving conditions, the range of $M_{z,unc}$ can be roughly determined [8]: $|M_{z,unc}| < M_{z,unc\_max}$.

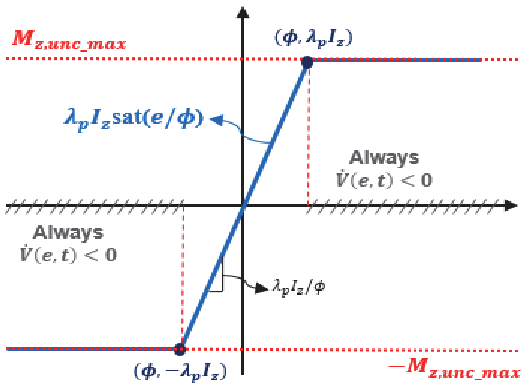

Fig.4. Visualization of feedback term $\lambda_P I_z \mathrm{sat}(e/\phi)$.

By substituting Eq. (13) into Eq. (14), the error dynamic equation is completed. Unlike the design process of general SMC, this paper suggests that the reference r_d replaces the state r in Eq. (14). This is to actively utilize r_d to generate a larger amount of feed-forward yaw moment. In doing so, the control input is derived as follows.

$$M_{z,des} = -(C_r l_r - C_f l_f)\beta + \frac{C_f l_f^2 + C_r l_r^2}{v_x} r_d \\ -C_f l_f \delta_f + I_z \dot{r}_d - \lambda_p I_z sat(e/\phi) \tag{15}$$

To prove the stability of Eq. (15), a Lyapunov function candidate $V(e)$, which is lower bounded, and its time derivative are given as follows.

$$V(e) = (1/2)\cdot e^2 \tag{16}$$

$$\dot{V}(e) = e \cdot \dot{e} \tag{17}$$

Substituting Eq. (14) into Eq. (17) yields Eq. (18).

$$\dot{V}(e) = -\frac{C_f l_f^2 + C_r l_r^2}{I_z v_x} e^2 - \frac{1}{I_z}\left[\lambda_p I_z sat(e/\phi) - M_{z,unc}\right] e \tag{18}$$

If $\lambda_P I_z < M_{z,unc\_max}$, there is no region of e that always satisfies $\dot{V}(e) < 0$.

On the other hand, if $\lambda_P I_z \geq M_{z,unc\_max}$, $\dot{V}(e) < 0$ (i.e. $\dot{V}(e)$ is negative semidefinite) is always satisfied in the region $|e| \geq \phi$, as shown in Fig. 4: $M_{z,unc\_max} = 2000\ Nm$ and $\lambda_P = M_{z,unc\_max}/I_z = 0.62$ in this paper. Therefore, e can be ultimately bounded by ϕ. Hence, if $\phi \to 0$, it can be shown that the tracking error e converges to 0 as $t \to \infty$ [23].

Considering that a high-gain feedback with too small ϕ may noticeably degrade the smoothness of the control action, an appropriately small value is selected as the boundary ϕ by cost-optimization techniques for gain tuning offline [24] (in this paper, $\phi = 0.04$).

In addition, it should be noted that replacing r in Eq. (14) with r_d eventually generates the negative term $-(C_f l_f^2 + C_r l_r^2)e^2/(I_z v_x)$ of $\dot{V}(e)$, which contributes to increasing the convergence rate of e in the region $|e| \geq \phi$. In other words, the resulting feed-forward term $(C_f l_f^2 + C_r l_r^2) r_d / v_x$ in Eq. (15) can improve both smoothness and convergence rate of control action.

IV. Torque Distribution

To generate the actual yaw moment corresponding to $M_{z,des}$, a method to distribute $T_{m,des}$ to each front wheel is presented in this section. In the case of existing methods for IWM torque distribution [1, 2, 3, 5, 6, 7, 8, 9, 10], the torque operation area is described only briefly. Also, some papers [1, 7, 8, 9] suggest torque distribution algorithms using an optimal allocation technique with constraints. However, to implement these in real-time, a numerical solver may cause relatively heavy computational burden because it runs iteratively several times per sample time. Under the condition that the control actuators are only two IWMs, a more practical and intuitive distribution method without any iterative calculation process would be appropriate for real-car application.

A. Maximum In-Wheel Motor Torque

The maximum IWM torques have to be determined from the tire friction circle. Firstly, the vertical tire forces at each front wheel can be expressed as follows:

$$\begin{bmatrix} F_{z,fl} \\ F_{z,fr} \end{bmatrix} = \frac{mg}{2L}\begin{bmatrix} l_r \\ l_r \end{bmatrix} + \frac{mha_x}{2L}\begin{bmatrix} -1 \\ -1 \end{bmatrix} + \frac{mha_y}{2t}\begin{bmatrix} -1 \\ 1 \end{bmatrix} \tag{19}$$

where h is the height of CG; t track width; and a_x the longitudinal acceleration at CG, respectively. Then, in order to obtain the lateral tire forces of the front left and right wheels, their ratio $F_{y,fl}/F_{y,fr}$ and sum $F_{yf}(= F_{y,fl} + F_{y,fr})$ are utilized. From Eq. (1) and Eq. (2), F_{yf} can be obtained as

$$F_{yf} = \frac{ml_r a_y + I_z \dot{r} - M_{z,des}}{L}. \tag{20}$$

From the equations of the lateral tire forces of front wheels in [6], their ratio is derived as follows:

$$\frac{F_{y,fl}}{F_{y,fr}} = \frac{F_{z,fl}}{F_{z,fr}}\left(\frac{v_x\beta + rl_f}{v_x - rt/2} - \delta_f\right) \Big/ \left(\frac{v_x\beta + rl_f}{v_x + rt/2} - \delta_f\right). \tag{21}$$

With the sum F_{yf}, $F_{y,fl}$ and $F_{y,fr}$ are obtained as

$$F_{y,fl} = F_{yf} / (1 + F_{y,fr} / F_{y,fl}) \tag{22}$$

$$F_{y,fr} = F_{yf} / (1 + F_{y,fl} / F_{y,fr}). \tag{23}$$

Assuming that F_x without braking is T_m/R_e, the maximum IWM torque from the tire friction circle is $R_e\sqrt{\mu^2 F_z^2 - F_y^2}$.

Another point to be noted is the T-N (torque-rotational speed) curve of IWM. this T-N curve presents an inverse relationship between the maximum available motor torque T_{m_TN} and the wheel speed v_w. In summary, the maximum IWM torque of each wheel is as follows ($i = fl, fr$):

$$T_{m\_\max,i} = \min(R_e\sqrt{\mu^2 F_{z,i}^2 - F_{y,i}^2}, T_{m\_TN,i}). \tag{24}$$

Here, T_{m_max} in Eq. (24) is regarded as a positive limit value considering both the electrical characteristics of IWM and the physical tire characteristics.

The state of charge of IWM battery can be recharged during most regenerative braking with a negative IWM torque [25, 26]. To avoid excessive overcharging of battery, it is recommended that the maximum regenerative torque T_{m,reg_max}, i.e. the negative limit value be set strictly, even if the maximum

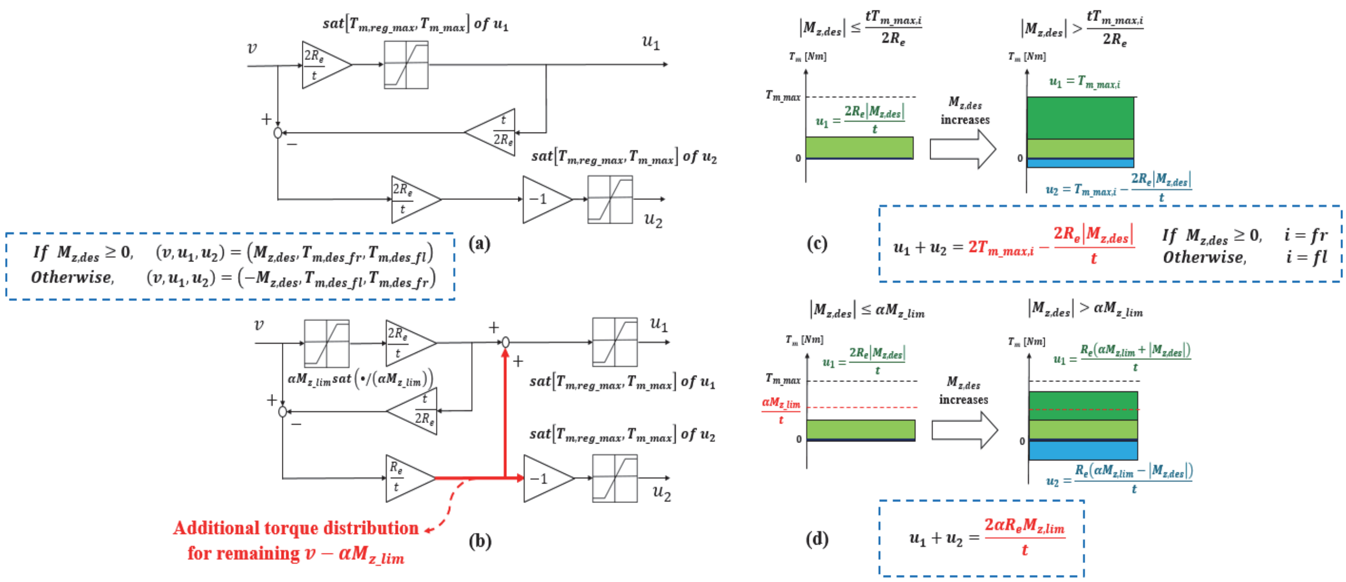

Fig. 5. Torque distribution based on Daisy-chaining allocation. Algorithm structure: (a) Conventional and (b) Proposed methods. Sum of torque inputs: (c) Conventional and (d) Proposed methods.

available yaw moment becomes small (T_{m,reg_max} is set to be a constant value of -200 Nm in this paper). Finally, the maximum available yaw moment is designed as follows.

$$M_{z\_\lim} = \begin{cases} t(T_{m\_\max,fr} - T_{m,reg\_\max,fl})/(2R_e) & \text{If } M_{z,des} \geq 0 \\ t(T_{m\_\max,fl} - T_{m,reg\_\max,fr})/(2R_e) & \text{otherwise} \end{cases} \quad (25)$$

For safety reasons, the desired yaw moment $M_{z,des}$ is limited to the following range: $M_{z,des} \sim [-M_{z\_lim}, M_{z\_lim}]$.

B. Daisy-Chaining Allocation

In the torque distribution between the two IWMs of the front wheels, it is desirable to operate only positive IWM torque: a large negative IWM torque at high wheel speed may cause deterioration of IWM durability [5]. However, in situations when a large amount of yaw moment is urgently required, use of both positive and negative IWM torques within the torque operation area is allowed. Daisy-chaining method for redundant actuators, which was first introduced in [27], is a quite effective allocation method to meet these requirements. Its key idea is described in the following. The relationship between the virtual v and actuator inputs u is given as follows.

$$v = B_1 u_1 + B_2 u_2 + \cdots + B_M u_M \quad (26)$$

If v is not satisfied by the first input u_1, the second input u_2 is generated to satisfy the remainder. In the same way, more than two inputs can be allocated to satisfy the virtual input. Therefore, the expressions of the conventional Daisy-chaining allocation are as follows:

$$\begin{aligned} u_1 &= sat_{u_1}\left(B_1^{-1} v\right) \\ u_2 &= sat_{u_2}\left(B_2^{-1}(v - B_1 u_1)\right) \\ &\vdots \\ u_M &= sat_{u_M}\left(B_M^{-1}(v - \sum_{k=1}^{M-1} B_k u_k)\right) \end{aligned} \quad . \quad (27)$$

In this section, the existence of the tuning parameter α makes a difference from the conventional Daisy-chaining allocation method. Figures 5 (a) and (b) show the structures of torque distribution based on conventional and proposed Daisy-chaining allocation methods, respectively. This $\alpha \in \{\alpha | 0 < \alpha \leq 1\}$ in Fig. 5 (b) determines when the second input u_2 will intervene.

Specifically, consider the situation when $M_{z,des} \geq 0$. If $v(= M_{z,des})$ requires a value less than αM_{z_lim}, only the first input $u_1 (= T_{m,des\_fr})$ is allocated. Conversely, if $v > \alpha M_{z\_lim}$, IWM torque corresponding to αM_{z_lim} is allocated to $u_1 (= T_{m,des\_fr})$ in advance. Then, to generate the additional yaw moment as much as the remaining $v - \alpha M_{z\_lim}$, $T_{m,des}$ corresponding to the remaining $v - \alpha M_{z\_lim}$ are divided into the left and right wheels with the same magnitude and different sign. In the case that $M_{z,des} < 0$, (v, u_1, u_2) is converted to $(-M_{z,des}, T_{m,des\_fl}, T_{m,des\_fr})$ and the same procedure as above is performed. Based on these findings, the torque distribution with the proposed Daisy-chaining allocation is derived as

$$T_{m,des\_fl} = \begin{cases} R_e(\alpha M_{z\_\lim} - M_{z,des})/t & (M_{z,des} < -\alpha M_{z\_\lim}) \\ -2R_e M_{z,des\_f}/t & (-\alpha M_{z\_\lim} \leq M_{z,des} < 0) \\ 0 & (0 \leq M_{z,des} \leq \alpha M_{z\_\lim}) \\ R_e(\alpha M_{z\_\lim} - M_{z,des})/t & (\alpha M_{z\_\lim} < M_{z,des}) \end{cases} \quad (28)$$

$$T_{m,des\_fr} = \begin{cases} R_e(\alpha M_{z\_\lim} + M_{z,des})/t & (M_{z,des} < -\alpha M_{z\_\lim}) \\ 0 & (-\alpha M_{z\_\lim} \leq M_{z,des} < 0) \\ 2R_e M_{z,des}/t & (0 \leq M_{z,des} \leq \alpha M_{z\_\lim}) \\ R_e(\alpha M_{z\_\lim} + M_{z,des})/t & (\alpha M_{z\_\lim} < M_{z,des}) \end{cases} . \quad (29)$$

In the torque distribution of IWM, the advantages of the proposed Daisy-chaining allocation method in comparison with the conventional one are summarized as follows.

1) By adjusting α, it is possible to freely tune the timing of the negative IWM torque intervention.

2) The greater the magnitude of the sum of torque inputs, the greater the intervention in the change in vehicle longitudinal velocity, regardless of the driver's pedal command. As shown in Figs. 5 (c) and (d), the magnitude of the sum of torque inputs

in each Daisy-chaining allocation is as follows (if $M_{z,des} \geq 0$, $i = fl$ and otherwise, $i = fr$).

$$\text{Conventional:} \quad \left|u_1 + u_2\right| = 2\left|T_{m\_\max,i} - R_e\left|M_{z,des}\right|/t\right| \tag{30}$$

$$\text{Proposed:} \quad \left|u_1 + u_2\right| = 2\alpha R_e M_{z,\lim}/t \tag{31}$$

In case of $\alpha \leq \left|\frac{tT_{m\_max,i}}{R_e M_{z,lim}} - \frac{|M_{z,des}|}{M_{z,lim}}\right|$, Eq. (31) becomes smaller than Eq. (30). This is an advantage of the proposed allocation: it is less involved in the longitudinal velocity command of the driver.

V. Simulation Study

Prior to the experiments, simulation studies were conducted to verify the superiority of the proposed SMC algorithm. CARSIM, the vehicle dynamics software, and MATLAB/Simulink are utilized. The used vehicle model was an E-class sedan with the parameters of an actual luxury sedan: a Hyundai Genesis DH (refer to Table I). The powertrain architecture was a 4WD system consisting of IWMs in the front wheels and an engine driving the rear wheels. The tire model used was the Magic Formula tire model [28]. To fully exploit the potential of simulation, this TRFC is given as $\mu = 0.7$ in this section.

A. Modeling of In-Wheel Motor System

Both mechanical and electric equations of the IWM system are given as follows:

$$J_{w,eq}\dot{w}_m + B_{w,eq}w_m = T_m - T_{dist} \tag{32}$$

$$L_m\dot{i}_m + R_m i_m = v_m - k_b w_m \tag{33}$$

where the IWM torque T_m, ground disturbance torque T_{dist} and the motor angular speed w_m are as follows, respectively:

$$T_m = Nk_t i_m \tag{34}$$

$$T_{dist} = R_e(F_x + \mu_{rr}F_z) \tag{35}$$

$$w_m = \left(N/R_e\right)v_w. \tag{36}$$

Here, N is the total gear ratio of IWM (given as 8.74); k_t the motor torque constant; i_m the motor current; L_m the motor inductance; R_m the motor resistance; v_m the motor voltage; k_b the flux linkage; and μ_{rr} the rolling resistance coefficient of tire. Also, $J_{w,eq}$ and $B_{w,eq}$ are the moment of inertia and damping coefficient of the IWM system, respectively.

To model the IWM torque T_m in a loading situation, the transfer function between the desired and the actual IWM torques in the unloading test is preferentially derived by the empirical transfer function estimation (ETFE) [29]:

$$H_{unload}(s) = \frac{T_m(s)}{T_{m,des}(s)}. \tag{37}$$

In this unloading test free from the ground disturbance torque, data in the relatively high frequency domain over 5 Hz are not used for ETFE. As shown in Fig. 6, the estimated $H_{unload}(s)$ indicated by the blue solid line is closely matched to actual data under the 5 Hz frequency range. Lastly, in a loading situation involving the ground disturbance torque T_{dist}, the IWM torque

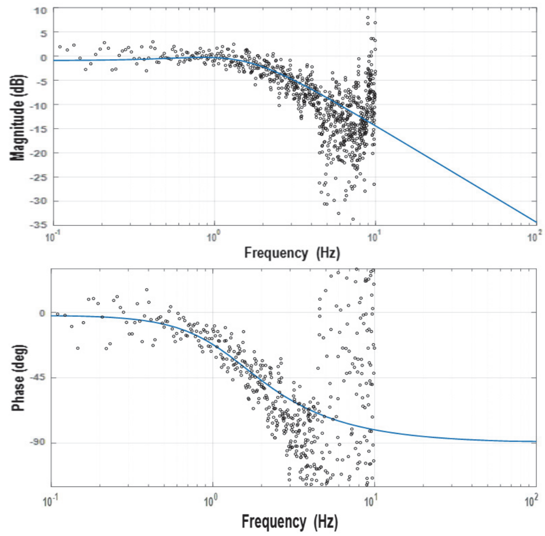

Fig.6. Bode plot of $H_{unload}(s)$. The black points and the blue solid line mean the actual and the estimated $H_{unload}(s)$, respectively.

T_m can be modeled by using Eqs. (32)-(37):

$$T_m(s) = e^{-t_d s}H_{unload}(s) \times \left(T_{m,des}(s) + \frac{k_b}{\left(J_{w,eq}s + B_{w,eq}\right)C(s)}T_{dist}(s)\right) \tag{38}$$

Here, $C(s)$ is the transfer function of the motor current controller (e.g. PI feedback type). A pure delay of t_d is caused by the gear backlash and the communication delay ($t_d = 0.02$ s in this paper). Finally, T_m generated from Eq. (38) is directly applied to the simulation vehicle.

B. Double Lane Change Test

A double lane change test, known as a representative method for evaluating vehicle cornering performance in extreme steering maneuvers, is performed on the simulation. Figure 7 (a) shows both the severe steering command and longitudinal velocity decelerating slowly from 80 km/h. Since the conventional controller (a proportional-integral-derivative (PID) controller tuned with the highest priority of yaw rate control accuracy) is also accompanied by same torque distribution algorithm, it is possible to clearly confirm the advantages of the smooth SMC compared with PID controller. These are as follows.

1) As shown in Fig. 7 (b), due to the feed-forward term, the proposed SMC leads to smoother and larger $M_{z,des}$ than the conventional one. In the case of the conventional PID controller, if P gain is further increased to increase the amount of desired yaw moment, the oscillatory torques of the conventional controller shown in Figs. 7 (c) and (d) are expected to become even more severe.

2) It can be seen in Fig. 7 (e) that the proposed SMC exhibits higher lateral acceleration under the same steering command due to larger $M_{z,des}$. This implies that the proposed SMC leads to higher vehicle cornering agility.

In a driving environment requiring high cornering agility, such as double lane change, these advantages of the proposed SMC algorithm can be of even greater benefit. Compared with other controllers except PID controller, the proposed smooth

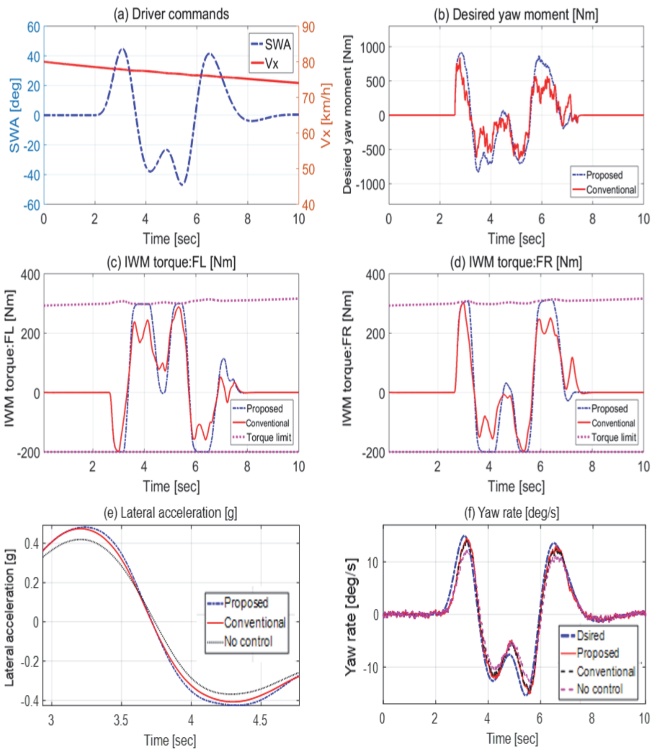

Fig. 7. Simulation results of the double lane change test.

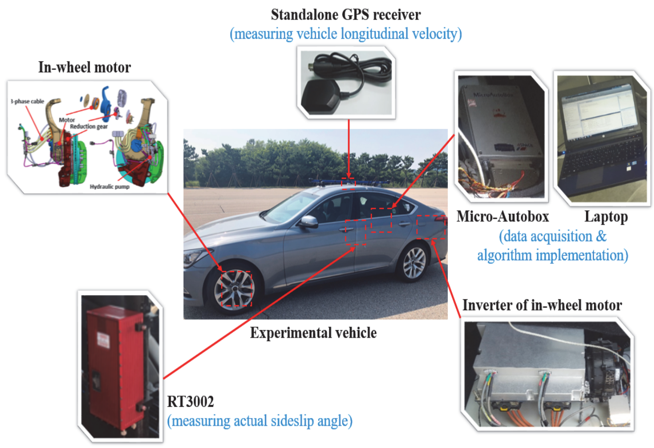

(a)

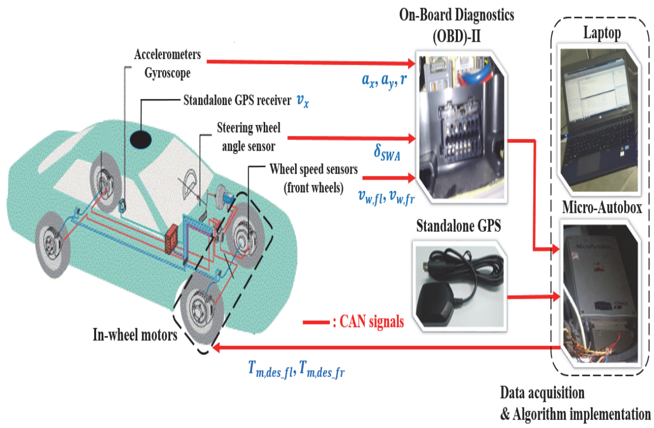

(b)

Fig. 8. Experimental environment: (a) Photographs and (b) Schematic diagrams of experimental set-up.

TABLE I
VEHICLE SPECIFICATIONS

Parameter	Quantity	Value
m	Total vehicle mass	2280 kg
l_f	CG-front axle distance	1500 mm
l_r	CG-rear axle distance	1510 mm
I_z	Yaw moment of inertia	$3234\ \mathrm{kg}\cdot m^2$
R_e	Effective tire radius	335 mm
h	Height of CG	550 mm
t	Track width	1600 mm
C_{f0}	Tire cornering stiffness of front axle (nominal)	140000 N/rad
C_{r0}	Tire cornering stiffness of rear axle (nominal)	150000 N/rad
GR_s	Steering gear ratio	21.1

SMC, which actively utilizes yaw rate reference information, is expected to have superiority especially in the smoothness of the control action.

VI. Experiments

The Hyundai Genesis DH (originally produced with a rear wheel drive system) equipped with IWM systems of the front wheels was used as an experimental vehicle. The maximum torque and power of the engine are 343.23 Nm and 211.5 kW, respectively. Excluding the total gear ratio N, those of IWM are 74.7 Nm and 23 kW, respectively.

In Fig. 8 (a), photographs of the experimental set-up are shown, such as experimental vehicle, standalone GPS, IWM, inverter, Micro-Autobox, Laptop, and RT3002 (for verification of sideslip estimation). This RT3002 from Oxford Technical Solutions is a high-precision differential GPS system, so that the sideslip angle measured by the RT3002 is regarded as an actual value. This device is located close CG of the vehicle. The standalone GPS receiver (to measure the vehicle longitudinal velocity) is mounted on the vehicle roof. The specifications of the experimental vehicle are presented in Table I.

The sampling time of each sensor is 1 ms for RT3002, 10 ms for in-vehicle sensors, and 50 ms for standalone GPS. Then, on the controller area network (CAN), the overall algorithm built into the Micro-Autobox runs with a sampling time of 10 ms. Figure 8 (b) illustrates the schematic diagrams of experimental set-up.

The driving test course on a high- μ road surface (μ~[0.9 1]) is located in the Hyundai-Kia R&D center, where GPS measurement is accurate due to the open-sky environment.

Since the driver directly manipulates the vehicle without the steering and pedal robots, the driver can feel the difference while steering in accordance with whether the control is intervening or not. From the experimental results with and without the proposed TV algorithm, its effectiveness in various driving scenarios is evaluated. All tuning parameters are set to be constant values.

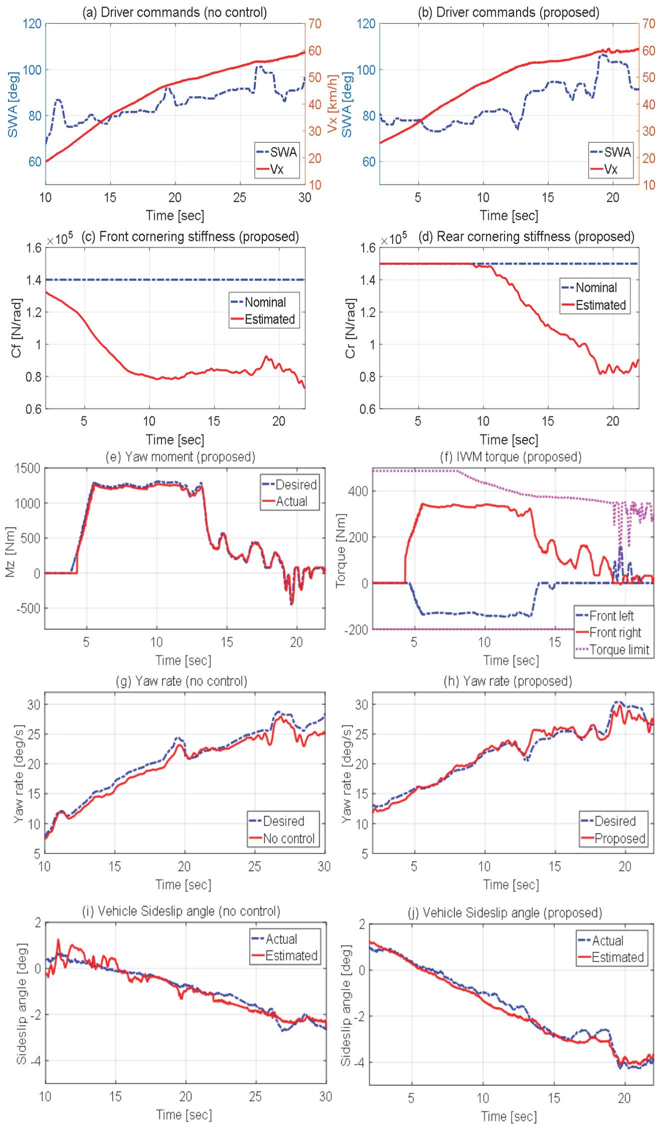

Fig. 9. Circle turn test results. Driver commands: (a) No control and (b) Proposed control. Estimated tire cornering stiffness (proposed): (c) Front and (d) Rear axles. (e) Yaw moment and (f) IWM torque with proposed control. Yaw rate: (g) No control and (h) Proposed control. Vehicle sideslip angle: (i) No control and (j) Proposed control.

A. Circle Turn Test (Steady State Cornering)

In the circle turn test, the driver manipulated the steering wheel to follow a circular track with a radius of 35 m. At the same time, by gradually stepping on the pedal from 20 km/h., the vehicle longitudinal velocity increased to 60 km/h. Figure 9 depicts the circle turn test results according to whether the proposed algorithm is applied or not. In Figs. 9 (e) and (f), yaw moments (desired $M_{z,des}$ and actual $M_{z,act} = t(T_{m,fr} - T_{m,fl})/(2R_e)$) and IWM torques of the front axle $T_{m,fl}$ and $T_{m,fr}$ are presented, respectively. The proposed algorithm is activated after 3 s, and the left and right IWM torques are distributed within the torque operation area $[T_{m,reg\_max}, T_{m\_max}]$. As the lateral tire force in the tire friction circle is saturated near 20 s, $R_e\sqrt{\mu^2 F_z^2 - F_y^2}$ is reflected in T_{m_max}, as shown in Fig. 9 (f).

Figures 9 (c) and (d) show $\hat{C}_f$ and $\hat{C}_r$ estimated by the EKF, respectively. After 10 s, $\hat{C}_r$ gradually decreases and this implies that the rear tire slip angle enters the tire nonlinear region. The magnitude of feed-forward term in $M_{z,des}$ decreases gradually after 10 s and the feedback term generates most of $M_{z,des}$ (see Fig. 9 (e)). From the desired and actual yaw rate signals in Figs. 9 (g) and (h), the difference in tracking performance depending on whether or not the control is applied can be confirmed.

As shown in Fig. 9 (e), within the low longitudinal velocity range between 5~15 s, the positive yaw moment improves the cornering agility with the actual yaw rate slightly exceeding the desired one. On the contrary, after 18 s (the high longitudinal velocity range), the negative yaw moment results in the enhancement of the cornering stability.

It can be seen that the magnitude of the sideslip angle in Fig. 9 (j) increases faster than that in Fig. 9 (i). This is further proof that the proposed algorithm leads to higher cornering agility with neutral-steering characteristics. As can be seen from the small difference between the estimated and actual values of the sideslip angle, the EKF has enough estimation accuracy to be utilized in the controller.

B. Skidpad Test (Steady State Cornering)

Next, the skidpad tests were performed to evaluate the vehicle behavior in the limit area of the tire grip; a vehicle driving on a circular track is slowly accelerated until the vehicle begins to slide out of the track. On the same circular track of the circle turn test, two skidpad tests having different initial steering wheel angles and initial longitudinal velocities were executed, respectively: 0 deg and 40 km/h in case 1 and 60 deg and 20 km/h in case 2. In Fig. 10, the under-steer characteristic curves (steering wheel angle versus lateral acceleration) of the skidpad tests are presented, which is one of the well-known indicators to evaluate cornering performance [1, 7, 8].

The following points should be noted in Fig. 10. First, in the linear lateral acceleration range of 0.2 to 0.6 g, the under-steer gradient (i.e. $\partial\delta_{SWA}/\partial a_y = (GR_s K_v)$) with the proposed algorithm is the lowest among the three kinds of data (refer to Table II): the conventional algorithm is the PID feedback controller. This result is because the proposed algorithm can generate more responsive and larger $M_{z,des}$ than the others due to the feed-forward term. Hence, the driver's steering effort required to exhibit the same lateral acceleration is further reduced with the proposed algorithm. It also represents improvement in the vehicle cornering agility.

Second, the maximum lateral acceleration $a_{y,max}$ that can follow the circular track increases (refer to Table II). The reason is a yaw damping effect of $M_{z,des}$ in the high lateral acceleration range ($a_y > 0.8\ g$). Therefore, even if the tire slip increases, $M_{z,des}$ can prevent the vehicle from sliding out of the track. This increase of maximum lateral acceleration means that the lateral tire forces of each front wheel are used as much as possible. Through the circle turn and skidpad tests, it is confirmed that the proposed algorithm contributes to the improvement of overall cornering performance at steady state cornering.

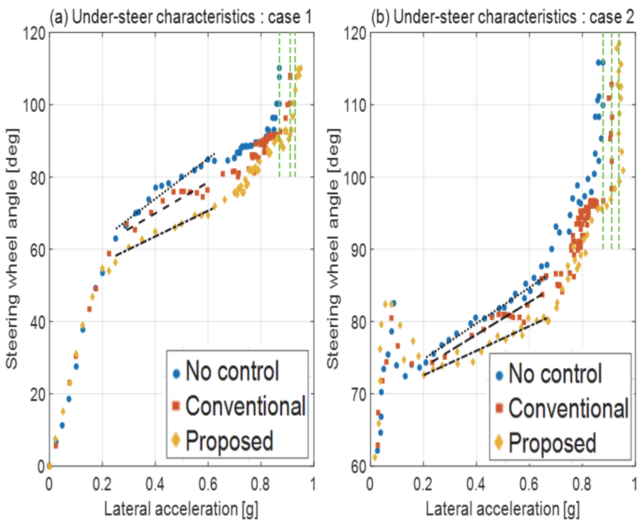

Fig. 10. Under-steer characteristic curves of skidpad test results: (a) Case 1 and (b) Case 2. The black dotted and the green dashed lines mean the under-steer gradient $\partial\delta_{SWA}/\partial a_y$ and the maximum lateral acceleration $a_{y,max}$, respectively.

C. Lane Change Test (Transient State Cornering)

As shown in Figs. 11 (a) and (b), with an initial vehicle longitudinal velocity of 75 km/h, the single lane change maneuver was performed to change lanes at a constant distance. The magnitudes of the lateral acceleration for the lane change in Figs. 11 (c) and (d) are similar regardless of the presence of TV algorithm. However, in no control case of Fig. 11 (a), it is shown that the driver needs more steering effort.

Figure 11 (h) shows IWM torques distributed to the left and right wheels appropriately within the torque operation area. As shown in Figs. 11 (i) and (j), the proposed algorithm improves the tracking performance of the yaw rate control. With the proposed algorithm, the yaw rate tracking becomes easier as the magnitude of the desired yaw rate r_d decreases (due to a reduction of the driver's steering effort). Also, the overshoots of the yaw rate at the cornering fade-out points near 9.3 s in Fig. 11 (j) are attenuated compared with those near 7.3 s in Fig. 11 (i). Similar to the results in the circle turn test, the estimated values of the sideslip angle are also accurate in this lane change test, as can be seen in Figs. 11 (k) and (L).

A comparison of yaw rate gradient is presented in Fig. 12. Figure 12 (a) points out the steering wheel angle versus the yaw rate at the start of the lane change in Fig. 11: for 4.4 ~ 6.2 s (no control) and for 6 ~ 8.2 s (proposed). In addition, a lane change test with the conventional PID controller was performed. As a result, the proposed algorithm yields the lowest yaw rate gradient $\partial\delta_{SWA}/\partial r$ with high yaw rate responsiveness and lag compensation effect (refer to Table II).

D. Sine Steer Test (Transient State Cornering)

Another transient state cornering, sine steer tests were conducted, as shown in Fig. 12 (b). Tests were within the yaw rate range of -15 to 15 deg/s, maintaining a constant longitudinal velocity of 55 km/h. The yaw rate gradient $\partial\delta_{SWA}/\partial r$ within the yaw rate range of -10 to 10 deg/s are illustrated in Fig. 12 (b): black solid lines (no control) and magenta dashed lines (proposed). Regardless of the sign of the

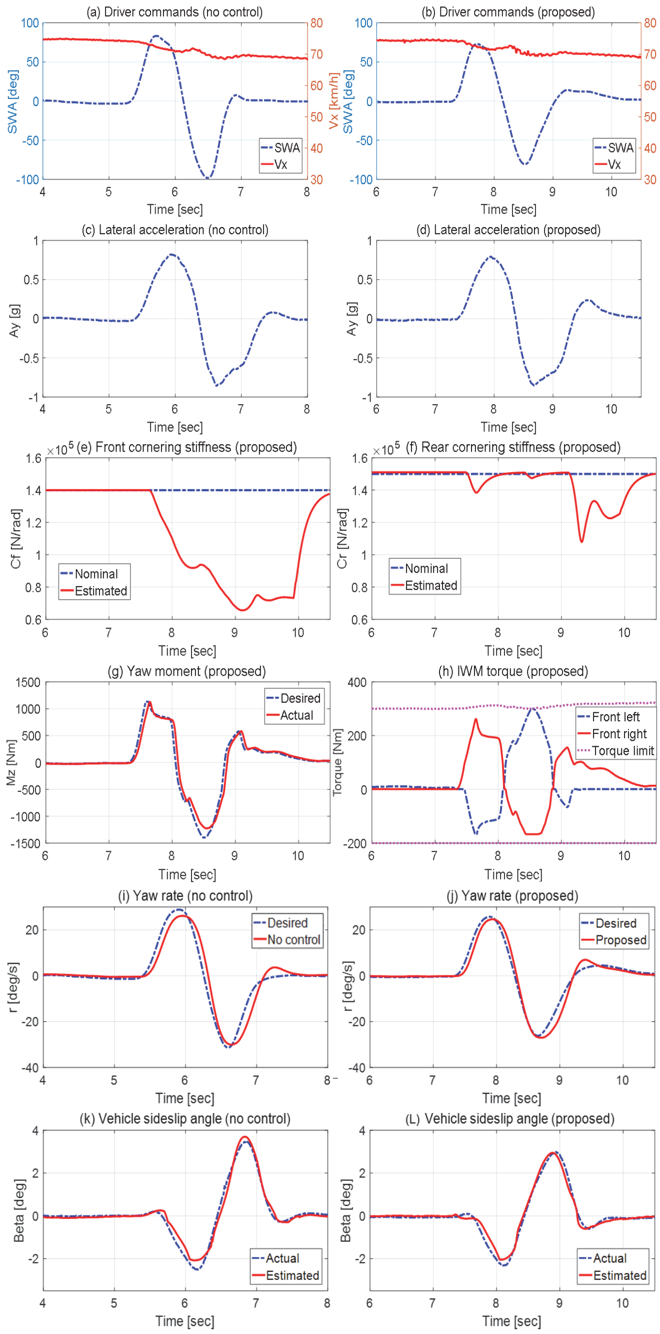

Fig. 11. Lane change test results. Driver commands: (a) No control and (b) Proposed control. Lateral acceleration: (c) No control and (d) Proposed control. Estimated tire cornering stiffness (proposed): (e) Front and (f) Rear axles. (g) Yaw moment and (h) IWM torque with proposed control. Yaw rate: (i) No control and (j) Proposed control. Vehicle sideslip angle: (k) No control and (L) Proposed control.

steering angle rate, the proposed algorithm exhibits the lowest $\partial\delta_{SWA}/\partial r$ among the three kinds of data, as shown in Table II. For visual reasons, the conventional PID controller is not displayed on Fig. 12 (b).

This low $\partial\delta_{SWA}/\partial r$ has the effect of reducing the hysteresis of the yaw rate response. At yaw rate points of -13 and 13 deg/s, sharper changes of the sign of steering angle rate are shown. The results of the yaw rate gradient in Fig. 12 claim that the proposed algorithm is certainly effective in improving the vehicle agility at transient state cornering.

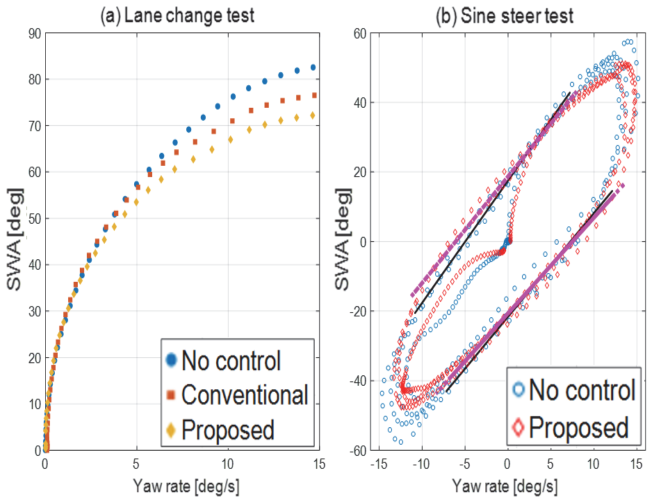

Fig. 12. Results of yaw rate response: (a) Lane change test and (b) Sine steer test. The black solid and the magenta dashed lines mean the yaw rate gradients $\partial\delta_{SWA}/\partial r$ in no control and proposed algorithm cases, respectively.

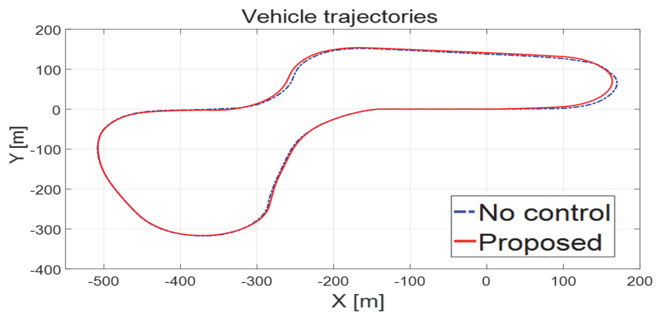

Fig. 13. Vehicle trajectories for closed-loop driving test.

E. *Closed-Loop Driving Test (Long Term Driving)*

The vehicle trajectories for this test are shown in Fig. 13, and there are some steep curve sections like usual racing courses (a maximum of 1 g of lateral acceleration is measured). Hence, it can be judged whether the proposed algorithm improves cornering performance even in a severe driving environment such as car racing. Some vehicle states and control results measured in this test are introduced in Fig. 14. As shown in Figs. 14 (a) and (b), the driver attempted to have a similar longitudinal velocity profile for each run, so that a lap time of about 1 minute was recorded on each run. When similar values of a_y exhibit, the proposed algorithm requires only a smaller steering effort, as seen in Figs. 14 (a)-(d).

Also, it is confirmed in Figs. 14 (e) and (f) that stable torque distribution is achieved without any problems even if IWM torques are continuously generated for a relatively long time. On the other hand, in the case of the conventional PID controller, the driver has difficulty completing the driving course due to the severe oscillation of IWM torque.

Lastly, in Figs. 14 (g) and (h), the root-mean-square error (RMSE) of yaw rate is reduced with the proposed algorithm (refer to Table II). From the results of the closed-loop driving test, it can be argued that the activation conditions, tuning gains and threshold values of the proposed TV algorithm are designed appropriately enough to be implemented for a relatively long time.

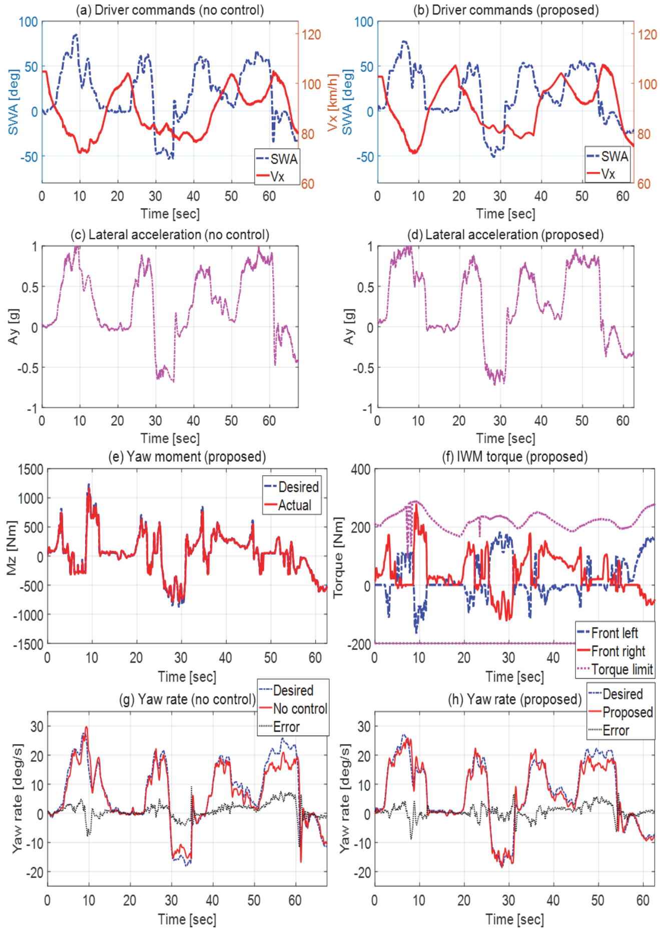

Fig. 14. Closed-loop driving test results. Driver commands: (a) No control and (b) Proposed control. Lateral acceleration: (c) No control and (d) Proposed control. (e) Yaw moment and (f) IWM torque with proposed control. Yaw rate: (g) No control and (h) Proposed control.

TABLE II
COMPARISON OF CORNERING PERFORMANCE

Test	Evaluation factor	Controller: No control	Controller: Conventional PID	Controller: Proposed SMC
Skidpad (case1)	$GR_s K_v$ [deg/g]	55.7	43.1	35.6
	$a_{y,max}$ [g]	0.87	0.91	0.93
Skidpad (case2)	$GR_s K_v$ [deg/g]	26.1	22.5	16.9
	$a_{y,max}$ [g]	0.88	0.91	0.93
Lane change	$\partial\delta_{SWA}/\partial r$ [s]	5.53	5.13	4.73
Sine steer	$\partial\delta_{SWA}/\partial r$ [s] ($\dot{\delta}_{SWA} > 0$)	3.51	3.3	3.06
	$\partial\delta_{SWA}/\partial r$ [s] ($\dot{\delta}_{SWA} < 0$)	2.98	2.91	2.75
Closed-loop driving	RMSE of yaw rate [deg/s]	2.76	N/A	2.17

VII. CONCLUSIONS

This paper proposes a novel torque vectoring algorithm for e-4WD vehicles equipped with in-wheel motor systems. The goal of the algorithm is to follow a yaw rate reference with neutral-steer characteristics leading to improved cornering agility. In this manner, the desired yaw moment is derived by a smooth sliding mode controller. Furthermore, the torque distribution method based on Daisy-chaining allocation is utilized, which cannot be found in existing TV algorithms.

Through real car-based experiments with various driving scenarios on a high- μ surface, it is confirmed that some evaluation factors in terms of the cornering performance are improved over the conventional PID controller as follows: improvements by 17.4 % and 2.2 % respectively in under-steer gradient and maximum available lateral acceleration at steady state cornering and 7.8 % in yaw rate gradient at transient state cornering. Finally, the RMSE of the yaw rate tracking error in long term driving is reduced by 21.4 % compared to the uncontrolled case. The main contributions of this study distinguished from the existing studies are as follows.

1) In the design process of the proposed smooth SMC, the feed-forward term actively reflects the yaw rate reference information to improve vehicle cornering agility. It also improves both smoothness and convergence rate of control action.

2) Daisy-chaining allocation is a practical and intuitive way to apply to redundant IWM actuators. Especially, the torque operation area is clearly described, which takes into account both the electrical characteristics of IWM and the tire friction circle.

3) Thanks to light computational burden, this algorithm is anticipated to be easily applicable to IWM-equipped vehicles to be mass-produced in the near future.

In conclusion, this research demonstrates that the proposed torque vectoring algorithm can be a meaningful solution to enhance the cornering performance of e-4WD vehicles equipped with in-wheel motor systems. Therefore, it is expected that even an ordinary driver can enjoy the fun-to-drive feeling and run corners as agilely as a skilled driver can. Compared with the conventional control method, the proposed algorithm has the shortcoming of requiring vehicle state estimation. Therefore, further research on the integration with the latest vehicle state estimation algorithms is needed.

Acknowledgment

This research was partly supported by the National Research Foundation of Korea (NRF) grant funded by the Korea government (MSIP) (No. 2017R1A2B4004116); the grant (20TLRP-C152478-02) from Transportation & Logistics Research Program funded by Ministry of Land, Infrastructure and Transport (MOLIT) of Korea government and Korea Agency for Infrastructure Technology Advancement (KAIA); the BK21+ program through the NRF funded by the Ministry of Education of Korea; and the Technology Innovation Program or Industrial Strategic Technology Development Program (10084619, Development of Vehicle Shock Absorber (Damper) and Engine Mount Using MR Fluid with Yield Strength of 60kPa) funded By the Ministry of Trade, Industry & Energy (MOTIE, Korea).

References

[1] L. Novellis, A. Sorniotti, and P. Gruber, “Wheel Torque Distribution Criteria for Electric Vehicles With Torque-Vectoring Differentials,” *IEEE Trans. Veh. Technol*., vol. 63, no. 4, pp. 1593-1602, 2014.

[2] Q. Lu, P. Gentile, A. Tota, A. Sorniotti, P. Gruber, F. Costamagna, and J. Smet, “Enhancing vehicle cornering limit through sideslip and yaw rate control,” *Mech. Sys. and Sig. Process.*, vol. 75, pp. 455-472, 2016.

[3] B. Ren, H. Chen, H. Zhao, and L. Yuan, “MPC-based yaw stability control in in-wheel-motored EV via active front steering and motor torque distribution,” *Mechatronics*, vol. 38, pp. 103-114, 2016.

[4] K. Han, M. Choi, B. Lee, and S. Choi, “Development of a Traction Control System Using a Special Type of Sliding Mode Controller for Hybrid 4WD Vehicles,” *IEEE Trans. Veh. Technol*., vol. 67, no. 1, pp. 264-274, 2018.

[5] S. Murata, “Innovation by in-wheel-motor drive unit,” *Vehi. Sys. Dyn*., vol. 50, no. 6, pp. 807-830, 2012.

[6] K. Nam, H. Fujimoto, and Y. Hori, “Lateral Stability Control of In-Wheel-Motor-Driven Electric Vehicles Based on Sideslip Angle Estimation Using Lateral Tire Force Sensors,” *IEEE Trans. Veh. Technol*., vol. 61, no. 5, pp. 1972-1985, 2012.

[7] D. Kasinathan, A. Kasaiezadeh, A. Wong, A. Khajepour, S. Che, and B. Litkouhi, “An Optimal Torque Vectoring Control for Vehicle Applications via Real-Time Constraints,” *IEEE Trans. Veh. Technol*., vol. 65, no. 6, pp. 4368-4378, 2016.

[8] T. Goggia, A. Sorniotti, L. Novellis, A. Ferrara, P. Gruber, J. Theunissen, D. Steenbeke, B. Knauder, and J. Zehetner, “Integral Sliding Mode for the Torque-Vectoring Control of Fully Electric Vehicles: Theoretical Design and Experimental Assessment,” *IEEE Trans. Veh. Technol*., vol. 64, no. 5, pp. 1701-1715, 2015.

[9] S. Fallah, A. Khajepour, B. Fidan, S. Chen, and B. Litkouhi, “Vehicle Optimal Torque Vectoring Using State-Derivative Feedback and Linear Matrix Inequality,” *IEEE Trans. Veh. Technol*., vol. 62, no. 4, pp. 1540-1552, 2013.

[10] S. Khosravani, A. Kasaiezadeh, A. Khajepour, B. Fidan, S. Chen, and B. Litkouhi, “Torque-Vectoring-Based Vehicle Control Robust to Driver Uncertainties,” *IEEE Trans. Veh. Technol*., vol. 64, no. 8, pp. 3359-3367, 2015.

[11] L. Zhang, H. Ding, Y. Huang, H. Chen, K. Guo, and Q. Li, “An Analytical Approach to Improve Vehicle Maneuverability via Torque Vectoring Control: Theoretical Study and Experimental Validation,” *IEEE Trans. Veh. Technol.*, vol. 68, no. 5, pp. 4514-4526, 2019.

[12] C. Chatzikomis, M. Zanchetta, P. Gruber, A. Sorniotti, B. Modic, T. Motaln, L. Blagotinsek, and G. Gotovac, “An energy-efficient torque-vectoring algorithm for electric vehicles with multiple motors,” *Mech. Sys. and Sig. Process.*, vol. 128, pp. 655-673, 2019.

[13] R. Hindiyeh and J. Gerdes, “A Controller Framework for Autonomous Drifting: Design, Stability, and Experimental Validation," *ASME J. Dyn. Syst., Meas., Control,* vol. 136, no. 5, pp. 051015, 2014.

[14] C. Coser, R. Hindiyeh, and J. Gerdes, "Analysis and control of high sideslip manoeuvres," *Vehi. Sys. Dyn*., vol. 48, pp. 317-336, 2010.

[15] G. Park, S. Choi, D. Hyun, and J. Lee, “Integrated Observer Approach Using In-vehicle Sensors and GPS for Vehicle State Estimation,” *Mechatronics*, vol. 50, pp. 134-147, 2018.

[16] R. Rajamani, *Vehicle Dynamics and control*, New York, NY, USA: Springer-Verlag, 2006.

[17] H. Her, Y. Koh, E. Joa, K. Yi, and K. Kim, “An Integrated Control of Differential Braking, Front/Rear Traction, and Active Roll Moment for Limit Handling Performance,” *IEEE Trans. Veh. Technol*., vol. 65, no. 6, pp. 4288-4300, 2016.

[18] G. Baffet, A. Charara, and D. Lechner, “Estimation of vehicle sideslip, tire force and wheel cornering stiffness,” *Control Engineering Practice,* vol. 17, pp. 1255-1264, 2009.

[19] M. Choi and S. Choi, "Linearized Recursive Least Square Methods for Real-time Identification of Tire-Road Friction Coefficient," *IEEE Trans. Veh. Technol*., vol. 62, no. 8, pp. 2906-2918, 2013.

[20] C. Lee, K. Hedrick, and K. Yi, "Real-time slip-based estimation of maximum tire-road friction coefficient," *IEEE Trans. Mechatronics*, vol. 9, no. 2, pp. 454-458, 2004.

[21] K. Han, E. Lee, M. Choi, and S. Choi, “Adaptive Scheme for the Real-Time Estimation of Tire-Road Friction Coefficient and Vehicle Velocity,” *IEEE Trans. Mechatronics*, vol. 22, no. 4, pp. 1508-1518, 2017.

[22] L. Li, J. Song, H. Li, D. Shan, L. Kong, and C. Yang, "Comprehensive prediction method of road friction for vehicle dynamics control," *IMechE Part D: J. Automobile Engineering,* vol. 223, pp. 987-1002, 2009.

[23] H. K. Khalil and J. Grizzle, *Nonlinear systems* vol. 3: Prentice hall New Jersey, 1996.

[24] K. Prabakar, "Gain tuning of proportional integral controller based on multiobjective optimization and controller hardware-in-loop microgrid setup" ph.D. dissertation, The University of Tennessee, Knoxville, Tennessee, USA, 2015.

[25] Y. Chen, X. Li, C. Wiet, and J. Wang, "Energy Management and Driving Strategy for In-Wheel Motor Electric Ground Vehicles With Terrain Profile Preview," *IEEE Trans. Ind. Inf.*, vol. 10, no. 3, pp. 1938-1947, 2014.

[26] J. Chen, C. Xu, C. Wu, and W. Xu, "Adaptive Fuzzy Logic Control of Fuel-Cell-Battery Hybrid Systems for Electric Vehicles," *IEEE Trans. Ind. Inf.*, vol. 14, no. 1, pp. 292-300, 2018.

[27] J. Buffington, and D. Enns, "Lyapunov stability analysis of daisy chain control allocation," *Journal of Guid., Con., and Dyn.,* vol. 19, no. 6, pp. 1226-1230, 1996.

[28] H. Pacejka, *Tire and vehicle dynamics.* Elsevier, 2005.

[29] A. Stenman, F. Gustafsson, D. E. Rivera, L. Ljung, and T. Mckelvey, "On adaptive smoothing of empirical transfer function," *Control Engineering Practice,* vol. 8, pp. 1309-1315, 2000.

Giseo Park received the B.S. degree in mechanical engineering from Hanyang University, Seoul, Korea, in 2014 and the M.S. and ph.D. degrees in mechanical engineering from Korea Advanced Institute of Science and Technology (KAIST), Daejeon, Korea in 2016 and 2020. His research interests include vehicle dynamics, control theory, active safety systems, autonomous driving system, and optimization.

Kyoungseok Han received the B.S. degree in civil engineering (minor in mechanical engineering) from Hanyang University, Seoul, Korea in 2013 and the M.S. and Ph.D. degrees in mechanical engineering from the Korea Advanced Institute of Science and Technology (KAIST), Daejeon, Korea in 2015 and 2018. He is currently a postdoctoral research fellow at the University of Michigan, Ann Arbor. His current research interests include vehicle dynamics and control, autonomous vehicle, battery electric vehicle, optimization, and control theory.

Kanghyun Nam received the B.S. degree in mechanical engineering from Kyungpook National University, Daegu, South Korea, in 2007, the M.S. degree in mechanical engineering from Korea Advanced Institute of Science and Technology, Daejeon, South Korea, in 2009, and the Ph.D. degree in electrical engineering from The University of Tokyo, Tokyo, Japan, in 2012. From 2012 to 2015, he was a Senior Engineer with Samsung Electronics Co., Ltd., Gyeonggido, South Korea. Since 2015, he has been an Assistant Professor in the School of Mechanical Engineering, Yeungnam University, Gyeongsan, South Korea. His research interests include motion control, vehicle

Heeseong Kim received the B.S degree in mechanical engineering from Yeongnam University, Gyeongsan, Korea, in 2017. He is currently working toward the M.S degree in automotive systems engineering from University of Michigan-Dearborn, Dearborn, USA. His research interests include motion control, vehicle dynamics and chassis control system.

Seibum B. Choi (M'09) received the B.S. degree in mechanical engineering from Seoul National University, Seoul, Korea; the M.S. degree in mechanical engineering from Korea Advanced Institute of Science and Technology (KAIST), Daejeon, Korea; and the Ph.D. degree in controls from the University of California, Berkeley, CA, USA, in 1993. Since 2006, he has been with the faculty of the Department of Mechanical Engineering, KAIST. His research interests include fuel-saving technology, vehicle dynamics and control, and active safety systems.